Role of storm track activity in the interannual seesaw of summer precipitation over northern Eurasia

Yoshiki Fukutomi and Kooiti Masuda
Frontier Research System for Global Change, JAMSTEC Yokohama Institute for Earth Sciences, Yokohama, Japan

Tetsuzo Yasunari
Hydrospheric Atmospheric Research Center, Nagoya University, Nagoya, Japan
Frontier Research System for Global Change, JAMSTEC Yokohama Institute for Earth Sciences, Yokohama, Japan

Received 25 June 2003; revised 7 October 2003; accepted 10 October 2003; published 30 January 2004.

[1] Oscillation between relatively dry and wet extremes is a noteworthy characteristic of the interannual variability in summer precipitation over Siberia. Recently, we identified an out-of-phase relationship in the temporal signature of basin-scale precipitation between eastern and western Siberia (ES and WS). This east-west seesaw has been especially pronounced during the past 30 years. The spatial structure of large-scale precipitation and circulation anomalies associated with this east-west seesaw is characterized by an east-west dipole across northern Eurasia. We extended our work to investigate the important atmospheric processes involved in the dipole patterns of precipitation and large-scale circulation anomalies for the northern summers (June–August) of 1972–2001. In particular, this work focuses on the role of storm track activities associated with synoptic-scale (<10 days) eddies in producing the stationary waves that correspond to the precipitation anomaly dipoles. Linear regression and composite analyses of various eddy statistics are performed for two contrasting extremes in the Siberian summer precipitation seesaw. These two extreme phases are denoted ES-wet-WS-dry and WS-wet-ES-dry. The summer mean atmospheric anomalies related to the precipitation seesaw show stationary wavetrain patterns in conjunction with the precipitation dipole anomalies. The cold trough/warm ridge dipole corresponds to the relative wet and dry region. Analysis of storm track activity reveals similar east-west contrasting structures, meaning that the displacements associated with the anomalous storm tracks are accompanied by a phase reversal between the two extreme phases. An anomalous stationary trough (ridge) corresponds to the anomalous high-(low-)synoptic-scale-eddy-activity region in both ES and WS. The forcing by synoptic-scale eddies is examined to confirm the storm track feedback on the Eurasian stationary waves. The results show that barotropic feedback induced by synoptic-scale eddy vorticity fluxes is in phase with the Eurasian wave field. Cyclonic (anticyclonic) circulation forcing is collocated with the anomalous stationary trough (ridge). These spatially coherent relationships suggest that storm track feedback due to eddy vorticity fluxes helps to reinforce and maintain the Eurasian wave structure coupled with the precipitation dipole pattern of each phase. Consequently, the interannual variability of the Eurasian storm track intensity and location is a crucial factor in forcing the mean precipitation and circulation patterns between the two extreme phases. *INDEX TERMS:* 1610 Global Change: Atmosphere (0315, 0325); 1620 Global Change: Climate dynamics (3309); 1655 Global Change: Water cycles (1836); 3319 Meteorology and Atmospheric Dynamics: General circulation; 3354 Meteorology and Atmospheric Dynamics: Precipitation (1854); *KEYWORDS:* storm track, interannual variability, precipitation

Citation: Fukutomi, Y., K. Masuda, and T. Yasunari (2004), Role of storm track activity in the interannual seesaw of summer precipitation over northern Eurasia, *J. Geophys. Res.*, *109*, D02109, doi:10.1029/2003JD003912.

1. Introduction

[2] Large-scale hydrological processes over northern Eurasia help to govern climate systems through atmosphere-ocean-land interactions and feedback (*Walsh* [2000], *Yang et al.* [2002], *Serreze et al.* [2003], *Fukutomi et al.* [2003], and others). For example, long-term variability in the summer hydrological cycle in northern Eurasia significantly affects the fresh water input into the Arctic Ocean, which in turn affects climate in adjacent lower

0148-0227/04/2003JD003912$09.00

latitudes. However, relatively few studies have investigated the characteristics of large-scale atmospheric circulations and the mechanisms forcing changes in the summer hydrological cycle in northern Eurasia.

[3] Our previous study [*Fukutomi et al.*, 2003] investigated the water balances in Siberian river basins and associated atmospheric fields and identified an east-west seesaw of dry and wet conditions as a marked characteristic of interannual variability of summer (June–August: JJA) precipitation in Siberia. They detected an out-of-phase relationship in the temporal signature of basin-scale precipitation with a 6- to 8-year cycle between eastern and western Siberia (hereafter ES and WS). This oscillatory tendency has dominated the area over the past 30 years. The spatial structure of large-scale precipitation, moisture transport, and circulation anomalies are all characterized by an east-west dipole pattern that spans northern Eurasia. This study posed a question; what are the dominant processes that might produce dipole variability in precipitation and concurrent stationary wave patterns?

[4] Over northern Eurasia, the Arctic frontal zone is well organized during the summer and is characterized by increased cyclogenic and frontal activity over the continent [e.g., *Serreze*, 1995; *Serreze et al.*, 2001]. The frontal location corresponds to the Eurasian portion of the summertime storm track activity in eddy variance statistics [e.g., *White*, 1982; *Blackmon and White*, 1982]. Greater storm track activity supports the formation of the summertime precipitation belt over northern Eurasia [*Serreze et al.*, 2003]. The interannual variability in Siberian summer precipitation may be related to interannual modulation in storm tracks. Stronger and weaker storm activity will result in above- and below-normal Siberian summer precipitation, respectively. In other words, changes in the mean circulation patterns associated with the east-west precipitation seesaw over Siberia may be related to changes in storm track activities over northern Eurasia. Past observational and modeling studies have suggested that representative teleconnection patterns in monthly or seasonal mean flow fields are strongly linked to storm track activities. High-frequency transient eddies (at synoptic and submonthly scales) generally act to reinforce and maintain the large-scale stationary flows of teleconnection patterns in regions of major storm tracks [e.g., *Lau*, 1988; *Lau and Nath*, 1991; *Ting and Lau*, 1993; *Hurrell*, 1995; *Sheng et al.*, 1998]. Therefore it seems reasonable to suppose that storm track feedback can reinforce and maintain also summer stationary waves coupled with the Siberian precipitation dipole patterns.

[5] This study sought to identify the atmospheric processes responsible for maintaining Eurasian waves associated with the Siberian precipitation dipole pattern. This study extends previous work, and focuses on storm track feedback on the seasonal mean circulations for extreme phases in the precipitation seesaw. Assessing the impact of synoptic-scale eddy forcing associated with storm track activities will help determine the physical mechanisms controlling the summer hydrological cycle in northern Eurasia. First, we document features in the spatial-temporal structure of these phases and link them to observational evidence given by *Fukutomi et al.* [2003]. Then, we illustrate the corresponding mean circulation pattern and storm tracks for Northern Hemisphere JJAs from 1972–2001. Eddy variance statistics on synoptic-scale perturbation timescales (1–10 days) capture the summertime storm track activity as it relates to the precipitation seesaw. Finally, we examine the storm track feedback on the summer stationary flow at the extreme phases of the seesaw. To achieve this, we use diagnostic techniques suggested by *Lau and Holopainen* [1984], *Lau and Nath* [1991], and others (see section 5 for details) and calculate the eddy vorticity and thermal forcing terms. These constitute the geopotential height tendency and the thermodynamic equations, respectively. We then use linear regression and the composite method to compare anomalous spatial structures in stationary flow patterns with the eddy statistic fields to determine the influence of synoptic-scale eddies on the formation of stationary waves over northern Eurasia.

[6] This paper is organized as follows: Section 2 briefly describes data sets and processing. Section 3 addresses statistical aspects of the interannual variability of summer precipitation in Siberia. Section 4 presents the large-scale atmospheric patterns and storm track activities. Section 5 discusses the storm track feedback based on the dynamical framework. Section 6 includes a summary and discussion.

2. Data Sources and Processing

[7] The global land precipitation data set produced by the National Oceanic and Atmospheric Administration (NOAA) Climate Prediction Center (CPC) is used to describe the large-scale precipitation variability in Siberia. The data set is called PREC/L: the gauge-based analysis of monthly precipitation over the global land areas [*Chen et al.*, 2002]. This precipitation analysis has been constructed on a 2.5° latitude/longitude grid using the optimal interpolation technique applied to gauge observations at over 15000 stations. The analysis has been updated for an extended period longer than 50 years from 1948 to the present at the NOAA/CPC. This study uses a record for the 54-yr period from 1948 to 2001.

[8] The National Centers for Environmental Prediction (NCEP)-National Center for Atmospheric Research (NCAR) reanalysis data set [*Kalnay et al.*, 1996; *Kistler et al.*, 2001], obtained from the NOAA Climate Diagnostics Center (CDC), is used to examine large-scale atmospheric patterns and storm track signatures associated with the Siberian precipitation variability. This data set includes pressure level analyses on a global 2.5° latitude/longitude grid. Data used in this study are daily and monthly geopotential height (z), temperature (T), zonal and meridional wind (u, v), and sea level pressure (SLP) fields for the 30-yr period from 1972–2001.

[9] This study focused on summertime storm track activity over northern Eurasia. To diagnose storm track activity, daily variables that retain synoptic-scale fluctuations with timescales shorter than 10 days are analyzed using a high-pass Butterworth filter developed by *Kaylor* [1977]. Then, various eddy statistics are calculated from time-filtered eddy components as described in the following sections. Daily perturbations of the variables are computed by subtracting the climatological seasonal cycle from the raw 365-day time series for each year before filtering. The climatological seasonal cycle is defined as the sum of the annual mean and the first three harmonics of the daily climatological-

mean values (30-yr average of each respective calendar day) at each grid point. This study only incorporates data for JJA. Final products are computed as 10-day high-pass filtered anomalies after removing the JJA mean values in individual years.

[10] A number of past studies that examined synoptic-scale baroclinic disturbances in the midlatitudes and high latitudes have used band-pass filters that retain timescales of 2.5–6 days [*Blackmon*, 1976] or 2–8 days [*Trenberth*, 1991]. Our study applies a high-pass filter with a cutoff period of 10 days to the time series of each perturbation quantity. This broader filter is more appropriate for capturing long-lived, slowly moving synoptic systems. Summertime synoptic-scale disturbances in northern Eurasia have periodicities of 8 to 10 days, which is a longer timescale than for synoptic-scale disturbances in the North Pacific and North Atlantic storm tracks, as noted by *Chang and Yu* [1999].

3. An Interannual East-West Seesaw in Summer Precipitation Over Siberia

[11] Our previous paper discussed the basic statistical features of the interannual variability of summer precipitation over Siberia. In this section, we reconfirm the principal mode of precipitation variability, and show results from statistical analyses to define an objective index that will be used for linear regression and composite analysis in the subsequent sections.

[12] Figure 1a is a time series of the interannual anomaly of the summer precipitation index for the East and West Siberian domains (shown in Figure 2) which is the same plot as Figure 9b of *Fukutomi et al.* [2003]. The ES (WS) precipitation index is the JJA precipitation anomaly averaged over the box bounded by 95°–135°E, 50°–70°N (55°–95°E, 50°–70°N). These time series appear to be out-of-phase with each other after the 1970s, which suggests an east-west seesaw in relative dry and wet regions over Siberia. To test this out-of-phase relationship, we calculated 21-year sliding correlation between ES versus WS precipitation index of Figure 1a. The result (Figure 1c) shows a strong negative correlation above 95% significant level during 1969–1989.

[13] For the regression and composite analysis, we construct a unified precipitation index that incorporates the out-of-phase nature of the ES and WS precipitation variability (Figure 1b). This index, the Siberian Precipitation Seesaw Index (hereafter SPSI), is the first principal component (PC1) obtained from the empirical orthogonal function (EOF) analysis of the JJA precipitation anomalies for 1948–2001 over the Siberian domain (see the green rectangle in Figure 2). The SPSI is derived as follows: Anomalous precipitation time series are meridionally averaged over latitudes 50°–70°N, for which the zonal distribution spans from 50°–140°E at a 2.5° grid interval. Then, an EOF analysis is performed on these longitudinally distributed anomalies. As a result, the leading EOF mode (EOF1) reflects an east-west seesaw pattern (not shown). As shown in Figures 1a and 1b, the SPSI increases during ES-wet-WS-dry phases and decreases during WS-wet-ES-dry phases. It is noted here that the EOF1 mode explains 29.6% of the total variance.

[14] Linear regression and composite methods are used in the following sections to identify the spatial pattern of elements associated with the wet and dry phases identified by the SPSI. Following our previous study [*Fukutomi et al.*, 2003], we employ the 30-yr period from 1971–2001 for the current analysis. Despite the decrease of absolute value of the sliding correlation from the late 1980s through the early 1990s (Figure 1c), we include the period after early 1990s in the analysis period in order to choose sufficient number of precipitation seesaw events for the composite analysis.

[15] The five most extreme positive (negative) events for the ES-wet-WS-dry (WS-wet-ES-dry) phase based on the SPSI in combination with the ES and WS precipitation index are used to construct the composite. The five ES-wet-WS-dry summers are 1974, 1981, 1982, 1988, and 1989; the five WS-wet-ES-dry summers are 1979, 1986, 1992, 1996, and 2001) (Figure 1b). These are the major precipitation phases of high SPSI and low SPSI, respectively.

[16] Figure 2 shows the spatial pattern of precipitation anomalies regressed from a 30-year time series of the SPSI from 1972–2002. The figure captures the east-west dipole distribution during a high-SPSI (ES-wet-WS-dry) condition. The dipole pattern shows many similarities to that produced by a regression that used a basin-scale precipitation index for the Lena River basin [*Fukutomi et al.*, 2003]. The statistical significance of this pattern is confirmed at the 95% level using a standard t-test (not shown). Anomalous dry and wet regions in Siberia switch locations as the low-SPSI phase event develops. It should be noted here that the regression analysis result based on the 22-yr period when the sliding correlation is high (1969–1989) reproduce the similar pattern (not shown). *Ye* [2002, Figure 7a] also shows a similar precipitation dipole pattern over Eurasia. That pattern is a summer leading mode derived from a rotated EOF analysis. However, there is little discussion on that mode in the paper.

[17] Now, let us consider the composite patterns of precipitation based on the SPSI. Figure 3 displays composite fields for the two extreme phases and 30-yr summer mean climatology of precipitation. The climatological JJA mean precipitation field (Figure 3a) shows basically the similar distribution with the 17-yr (1979–1995) climatology presented by *Fukutomi et al.* [2003]. A band of precipitation exceeding 60 mm month^{-1} extends from Europe into central Siberia along 55°–65°N and another band with higher amount lies from the east of Lake Baikal to northeast Asia and the south of eastern Siberia. The composite for the high-SPSI (ES-wet-WS-dry) summers (Figure 3b) reveals an increase of precipitation to the above-normal values in central-eastern Siberia to the north of 60°N and a decrease of it to the below-normal values in western Siberia. In contrast, the composite for the low-SPSI (WS-wet-ES-dry) summers shows a striking increase over the entire western Siberia and a decrease in eastern Siberia. The difference in absolute precipitation between high- and low-SPSI composites (Figure 3d) well captures the Siberian dipole pattern which is very similar to that in the regressed precipitation field (Figure 2). In relation to Figure 3d, composite percentage difference to the normal (climatological mean) precipitation value between the two phases is computed for the ES and WS domains. The resulting percentage is 27% for the ES domain and is 31% for the WS domain.

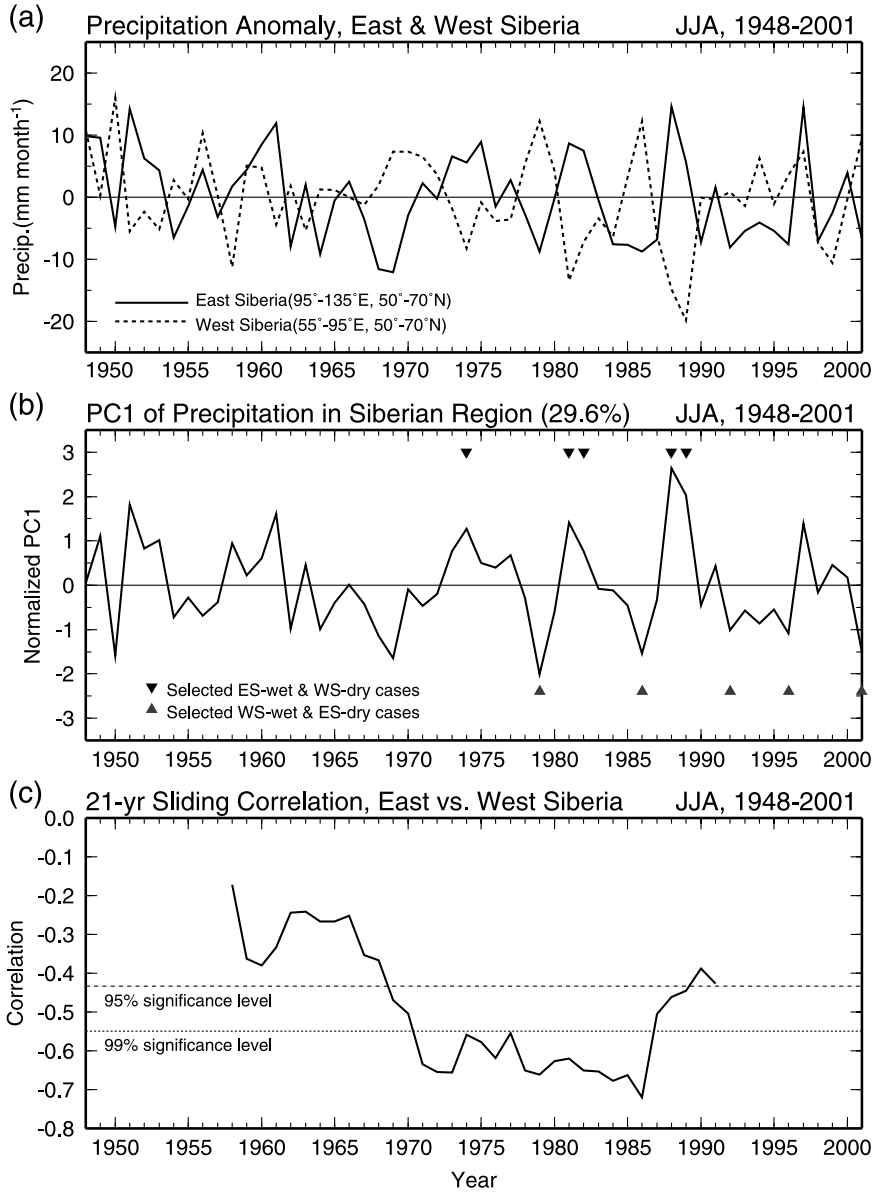

Figure 1. (a) Area-averaged precipitation index for JJA 1948–2001 (mm month^{-1}). Solid (dashed) line indicates the time series for the eastern (western) Siberian domain. The eastern (western) Siberian domain is enclosed by the grid box of 95°–135°E, 50°–70°N (55°–95°E, 50°–70°N). (b) First principal component (PC1) of precipitation anomalies in the broad Siberian domain (50°–140°E, 50°–70°N). (c) 21-year sliding cross correlation between the East and West Siberian precipitation index. The dashed lines indicate the 95% and 99% significance levels.

These facts also confirm the occurrence of the east-west oscillation of above-normal and below-normal precipitation condition in Siberia.

4. Large-Scale Atmospheric Patterns and Storm Track Activity Associated With the Precipitation Seesaw

4.1. Stationary Wave Patterns

[18] Basic atmospheric patterns related to the SPSI must be identified before discussing the role of storm track activity over northern Eurasia. Figure 4a shows the JJA mean 500-hPa geopotential height field regressed onto the SPSI. The polarity indicates a positive SPSI phase. A clear wave-train pattern with a zonal-wave number of about four extends from western Eurasia to the north Pacific. The east-west oriented dipole circulation structure across northern Eurasia is the upstream portion of this wavetrain. The wavetrain includes an anticyclonic center over the Ural Mountains-West Siberian Plain and a cyclonic center over the Central Siberian Plateau. A wave anomaly pattern of opposite sign occurs during the negative SPSI phase (not shown). These features are similar to those observed in a map of the leading rotated EOF mode of the NH 500-hPa z and maps of the regressed 500-hPa z based on the basin-scale precipitation index for the Lena and Ob rivers [cf. *Fukutomi*

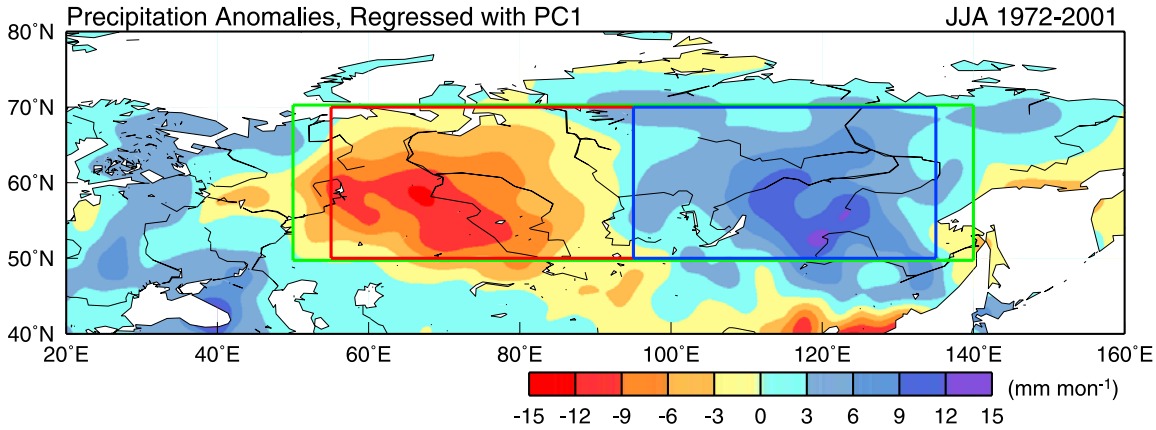

Figure 2. Spatial pattern of the JJA mean precipitation anomalies related to PC1 (mm month^{-1}). The eastern (blue), western (red) Siberian domain, and the broad Siberian domain for estimating PC1 (green) are shown.

et al., 2003]. *Serreze et al.* [2003] reported similar atmospheric patterns relating the interannual variability of precipitation minus evaporation for the Lena and Ob River basins. Regression maps of 300- and 850-hPa z associated with the SPSI also show good agreement with features in Figure 4a, suggesting a strong equivalent barotropic structure through the troposphere for this wave pattern.

[19] The 850-hPa temperature pattern (Figure 4b) shows troughs and ridges co-located with the 500-hPa z pattern. An anomalous cold (warm) core structure accompanies the trough (ridge) of the 500-hPa flow fields. Comparison of these patterns with Figure 2 reveals cyclonic (anticyclonic) and cold (warm) anomalies coupled with relative wet (dry) regions in northern Eurasia. This trough-ridge couplet is slightly upstream (west) from the precipitation dipole (Figure 2). Regression maps show that these wave anomalies over northern Eurasia and the north Pacific do not have a strong simultaneous connection to the Atlantic region signals.

4.2. Changes in the Storm Track Signature

[20] Transient eddy statistics were calculated using thirty 92-day summers to determine the spatial relationship between the storm track activity due to synoptic-scale eddies and the Siberian precipitation dipole pattern. The following variance statistics were used as measures of synoptic-scale eddy activity: mean standard deviation (SD) of 10-day high-pass filtered daily 500-hPa geopotential height (z'), sea level pressure (SLP′), 300-hPa meridional wind (v'), and the 850-hPa poleward heat flux due to synoptic-scale eddies ($\overline{T'v'}$). The prime denotes the 1–10-day perturbations and the overbar represents the seasonal average. Height anomalies z' are normalized using the factor sin 45°/sin ϕ, which is inversely proportional to the sine of latitude ϕ, before computing the SD. Such normalization makes z behave more like a geostrophic stream function. Statistics based on the normalized z' become more comparable with those based on the wind fields, as emphasized by *Wallace et al.* [1988].

[21] The 30-yr climatology of summer (JJA) storm tracks in northern Eurasia is shown in Figure 5. The distribution of the 500-hPa z' SD (Figure 5a) shows a region of high amplitude (enclosed by the 32-m contour) localized over western Siberia and adjacent Arctic coastal regions. The positions of these climatological maxima resemble those identified by eddy activity on subseasonal timescales [*White*, 1982] and 2.5–6 days [*Blackmon and White*, 1982] for the summer season. In contrast, a band of maximum transient variance at 300 hPa v' (Figure 5b) exceeding 8m s^{-1} covers a broad region from the north Atlantic to the Lena River basin (around 120°E) along 50°–65°N. The 850-hPa $\overline{T'v'}$ (Figure 5c) clearly shows low-level synoptic-scale eddy activity across northern Eurasia. A zonally stretched belt with maxima exceeding 3K m s^{-1} prevails over northern Eurasia. This agrees with the 11-yr July climatology of 2–8-day $\overline{T'v'}$ at 850 hPa plotted by *Raphael* [1997]. This marked band is distinct from the band over the north Atlantic or the north Pacific. The location of the well-organized Siberian storm track inferred from the statistics is coincident with the Arctic frontal zone [cf. *Serreze et al.*, 2001] and extra-tropical cyclone tracks [cf. *Whittaker and Horn*, 1984; *Chen et al.*, 1991] over northern Eurasia during summer.

[22] To determine how changes in storm track activity are associated with the interannual precipitation seesaw, it is necessary to regress the JJA mean SD of 500-hPa z' and SLP′ against the SPSI for the 30 years from 1972–2001. The results are displayed in Figures 6a and 6b, respectively. The anomaly signs in these maps correspond to a positive SPSI phase. The regression reveals a dipole-like structure in the zonal direction over northern Eurasia, although the positive anomaly centers over central-east Siberia for z' SD at 500-hPa are shifted westward about 15° relative to those in the SLP′ SD. In addition, these patterns are out-of-phase with the stationary waves (Figure 4) but are in phase with precipitation anomalies (Figure 2). Storm track activity increases over east-central Siberia and decreases over west Siberia in the high-SPSI phase, and vice versa in the negative SPSI phase (not shown). Positive (negative) anomalies identified by both SD maps almost lie over the positive (negative) precipitation anomalies in each phase.

[23] Composites of the storm track field defined by the 500-hPa z' SD anomalies (Figure 7) further highlight the difference in the structure of synoptic-eddy activity between the two precipitation extreme phases. As noted earlier, the

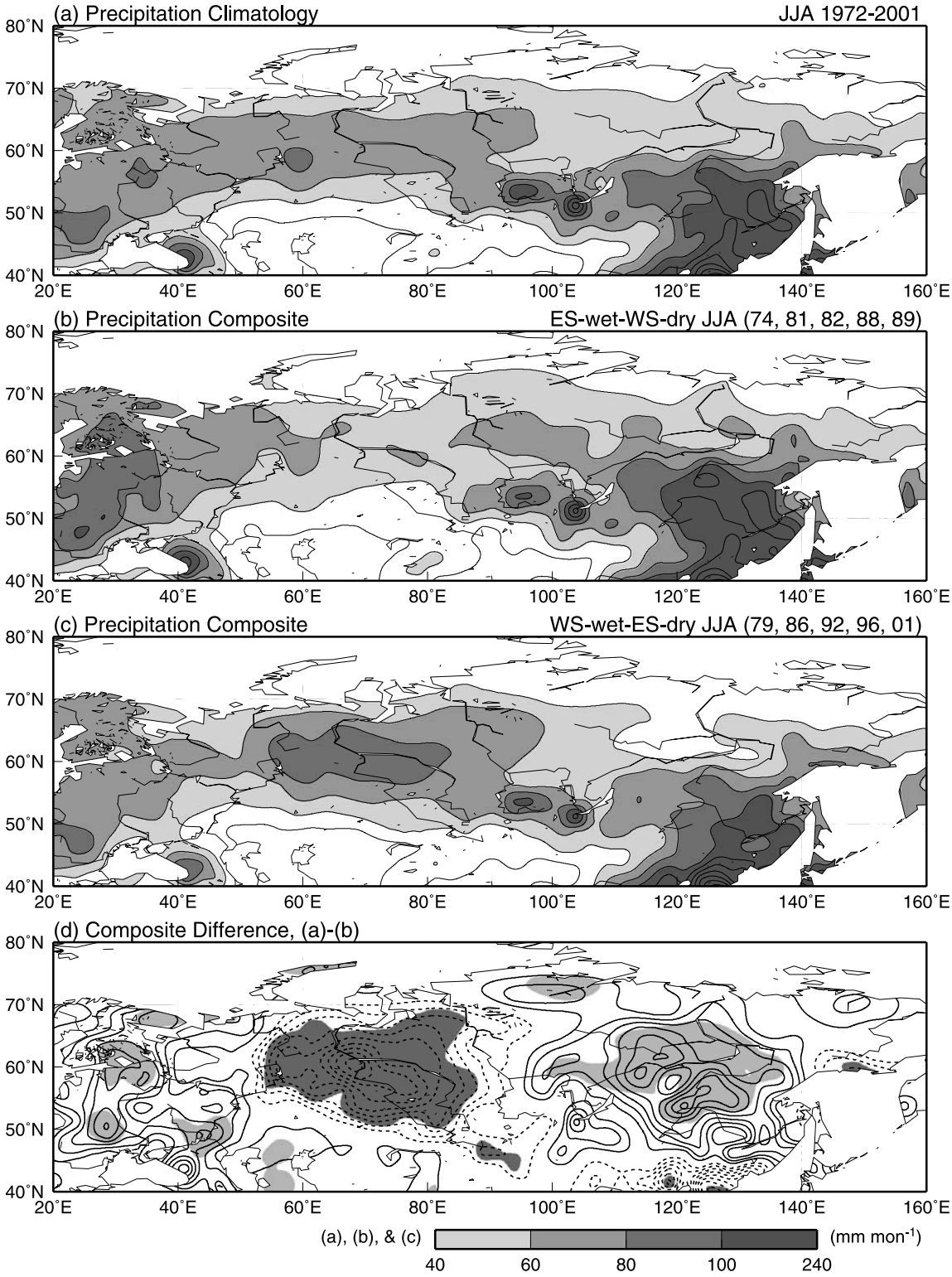

Figure 3. (a) Thirty-year (1972–2001) climatology of the JJA mean precipitation. Contour interval is 20 mm month^{-1}. Regions with values greater than 40 mm month^{-1} are shaded. (b) Composite of the JJA mean precipitation defined for the high-SPSI (ES-wet and WS-dry) phases (1974, 1981, 1982, 1988, and 1989). The definition of the contour interval and the shadings are same as those for Figure 3a. (c) Same as Figure 3b except for the low-SPSI (WS-wet and ES-dry) phases (1979, 1986, 1992, 1996, and 2001). (d) Composite difference between the two phases as defined by the high-SPSI composite minus the low-SPSI composite. Solid (dashed) contours indicate positive (negative) anomalies. Contour interval is 5 mm month^{-1}. Zero contours are omitted. Positive (negative) anomalies statistically significant at 90% level are lightly (darkly) shaded.

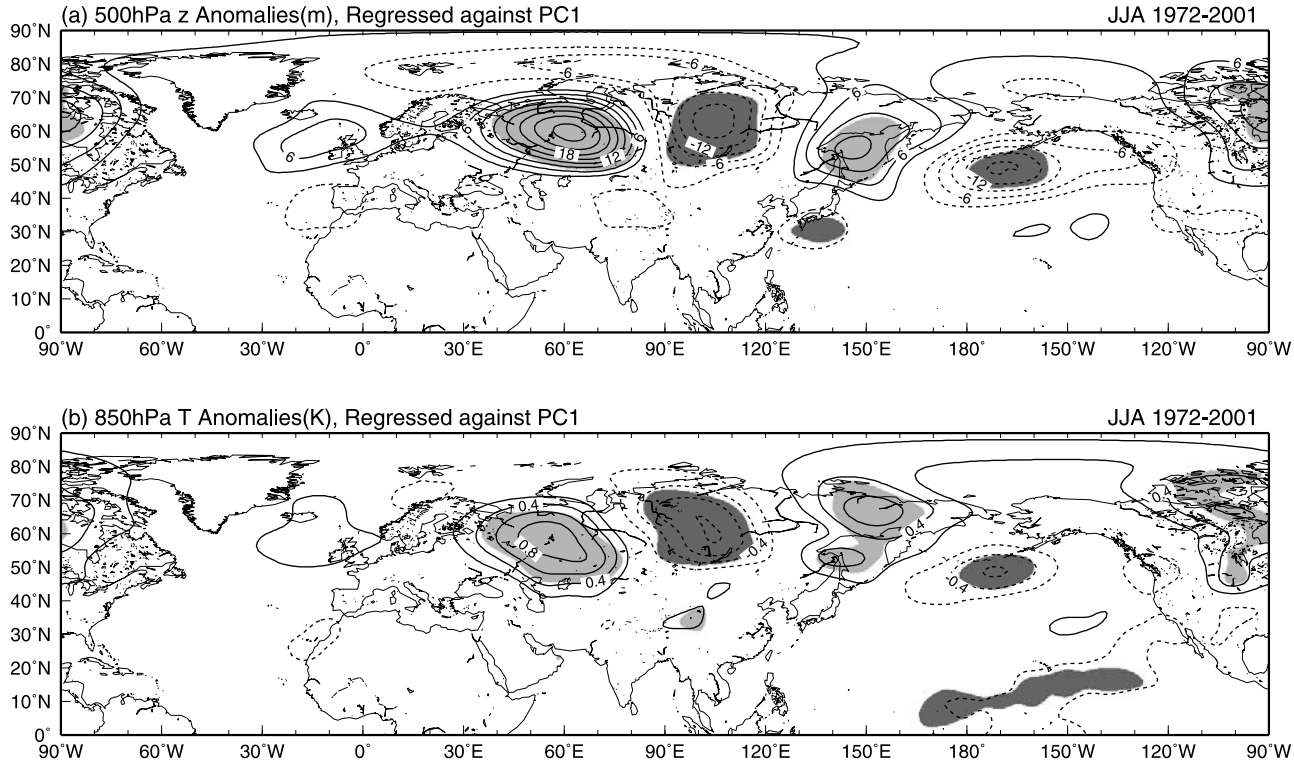

Figure 4. (a) Regression coefficient of the JJA-mean 500-hPa height anomalies with PC1 for JJA 1972–2001. Shaded regions indicate significance on the 95% level according to t-test. Solid (dashed) contours show the positive (negative) values. Zero contours are omitted. Contour interval is 3 m. (b) Same as Figure 4a except for the 850-hPa temperature anomalies. Contour interval is 0.2 K.

composites use two precipitation extreme phases: the highest-SPSI (ES-wet-WS-dry) summers (1974, 1981, 1982, 1988, and 1989) and the lowest-SPSI (WS-wet-ES-dry) summers (1979, 1986, 1992, 1996, and 2001). These composites are defined as departures from the climatological mean SD field (as in Figure 5a).

[24] In the high-SPSI phase (Figure 7a), maximum positive values with the 90% statistically significance level occur along the Arctic coast of central-eastern Siberia to the north of about 60°N, and extend southward over the western half of the Lena River basin. On the other hand, negative values spread over western Siberia although the coverage of the local statistically significant area is smaller. The composite in the low-SPSI phase (Figure 7b) reveals a nearly out-of-phase pattern over northern Eurasia to that in Figure 7a. The maxima with high positive values extend from northwest European Russia to the south of western Siberian Plain. Besides a band of significant negative values replace the positive one over the central-eastern Siberia in the opposite phase (Figure 7a). The difference field of the two composites (high-SPSI minus low-SPSI, Figure 7c) is spatially similar to the regressed pattern in Figure 6a. The east-west dipole pattern is also present. Composite maps of the SLP′ SD field were produced as in Figure 7 (not shown); the resulting patterns show many similarities with those of the 500-hPa z' SD field. These features confirm the displacement of the relative high and low storm track activity associated with the east-west alternation of relative dry and wet regions.

[25] In summary, there is a strong east-west contrast in anomalous activities of synoptic systems in two extreme phases of the precipitation seesaw. Linear regression and composite patterns show that positive (negative) SD anomalies are roughly collocated with positive (negative) anomalies of the precipitation dipole. This spatial relationship suggests that longitudinal displacement of relatively enhanced (reduced) storm track activity leads to high (low) precipitation anomalies in each phase. Systematic changes in storm track activity reflect a geographical change in the primary path of synoptic-scale precipitating systems over northern Eurasia. The stationary wave trough (ridge) over Eurasia enhances (reduces) storm track activity. Therefore the redistributed synoptic-eddy activity associated with the storm track shift may play an important role in creating the summer stationary wave pattern accompanying the east-west precipitation dipole.

5. Synoptic-Scale Eddy Forcing in the Summer Stationary Waves Associated With the Precipitation Seesaw

[26] Evidence from the regression and the composite maps of variance statistics suggests a spatially coherent relationship between the summer stationary waves and storm tracks in two contrasting precipitation phases. The next section considers dynamic forcing due to a synoptic-scale eddy flux to evaluate whether the systematic change in synoptic-scale eddy activity that occurs within a storm track

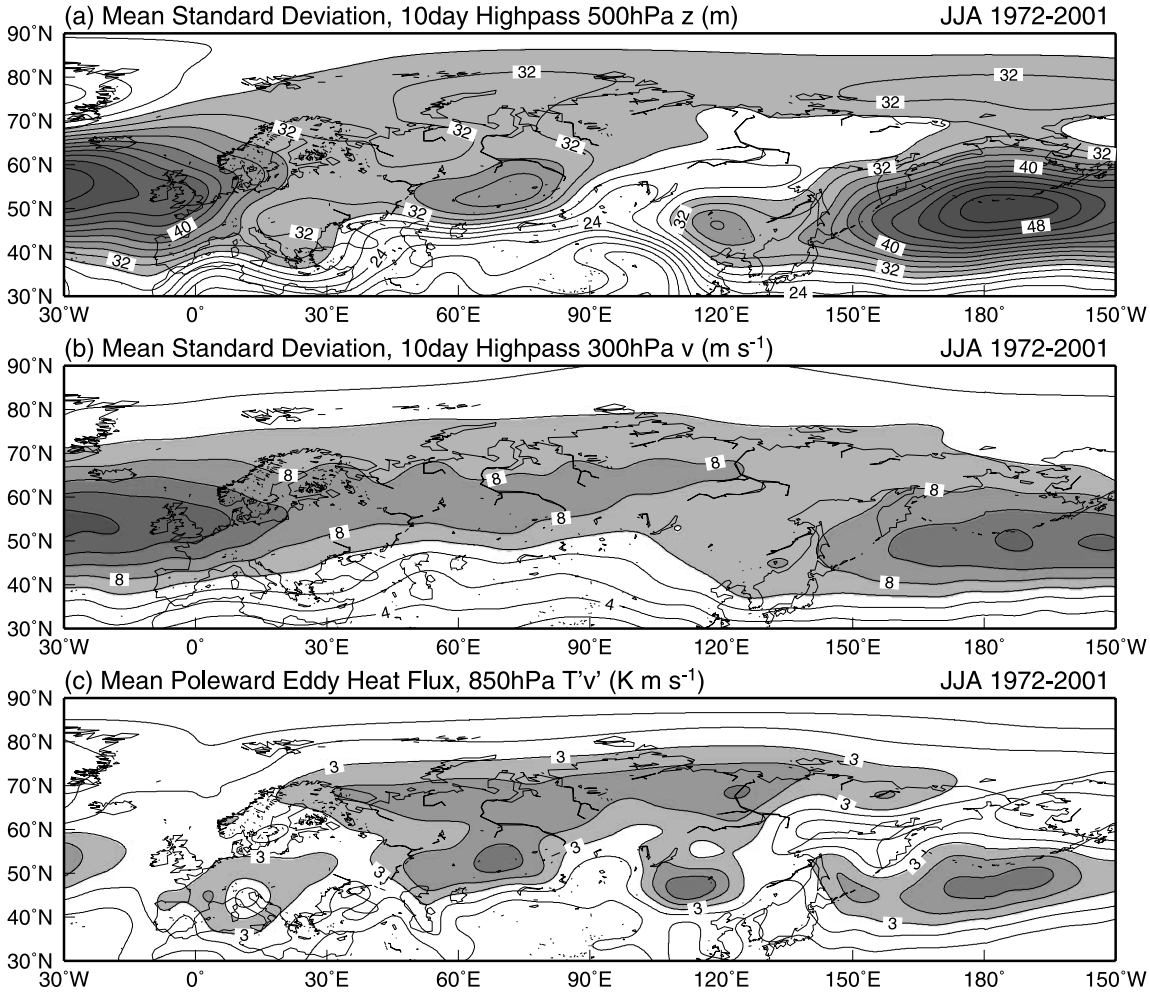

Figure 5. (a) Mean standard deviation (std dev) of 10-day high-pass filtered 500-hPa height for JJA 1972–2001. Contour interval is 2 m. Regions with std dev greater than 30 m are shaded. (b) Same as Figure 5a but for the 300-hPa meridional wind. Contour interval is 1 m s^{-1}. Regions with std dev greater than 7 m s^{-1} are shaded. (c) Synoptic-scale transient eddy heat flux at 850 hPa averaged over the same period. Contour interval is 1 K m s^{-1}. Regions with values greater than 3 K m s^{-1} are shaded.

helps to reinforce and maintain the anomalous stationary flow for each phase.

5.1. Geopotential Height and Temperature Tendencies Induced by Transient Eddies

[27] The effects of vorticity and thermal forcing by synoptic-scale eddies on the mean flow are calculated using methods introduced by *Lau and Holopainen* [1984] and *Lau and Nath* [1991]. They defined barotropic and baroclinic eddy feedbacks to the mean flow that are represented by geopotential height and temperature tendencies in terms of the convergence of eddy vorticity and heat fluxes. The (barotropic) eddy vorticity forcing expressed as a height tendency is

$$\frac{\overline{\partial z}}{\partial t} = -\frac{f}{g}\nabla^{-2}\left[\boldsymbol{\nabla}\cdot\left(\overline{\zeta'\mathbf{V}'}\right)\right], \tag{1}$$

[28] Where, ζ is the relative vorticity; $\mathbf{V}$ is the horizontal wind vector; f is the latitudinally dependent Coriolis parameter; and g is the gravitational acceleration. The other notation is the same as that used in the variance statistics. The (baroclinic) eddy thermal forcing expressed as a temperature tendency is

$$\frac{\overline{\partial T}}{\partial t} = -\nabla\cdot\left(\overline{T'\mathbf{V}'}\right). \tag{2}$$

[29] Using these equations, *Lau* [1988] and *Lau and Nath* [1991] demonstrated that synoptic-scale eddy activity associated with the large-scale changes in storm tracks reinforces anomalous monthly flow patterns over the North Pacific and the North Atlantic during winter. Many subsequent observational studies applied the same or similar formulas to investigate interactions between transient eddies and NH winter teleconnection patterns, like the Pacific-North American (PNA) and the North Atlantic Oscillation (NAO) pattern (*Klasa et al.* [1992], *Trenberth and Hurrell* [1994], *Sheng et al.* [1998], *Hurrell* [1995], *Hurrell and van Loon* [1997], and others).

[30] These formulas can be used as a diagnostic of storm track feedback to explain possible causes of the stationary

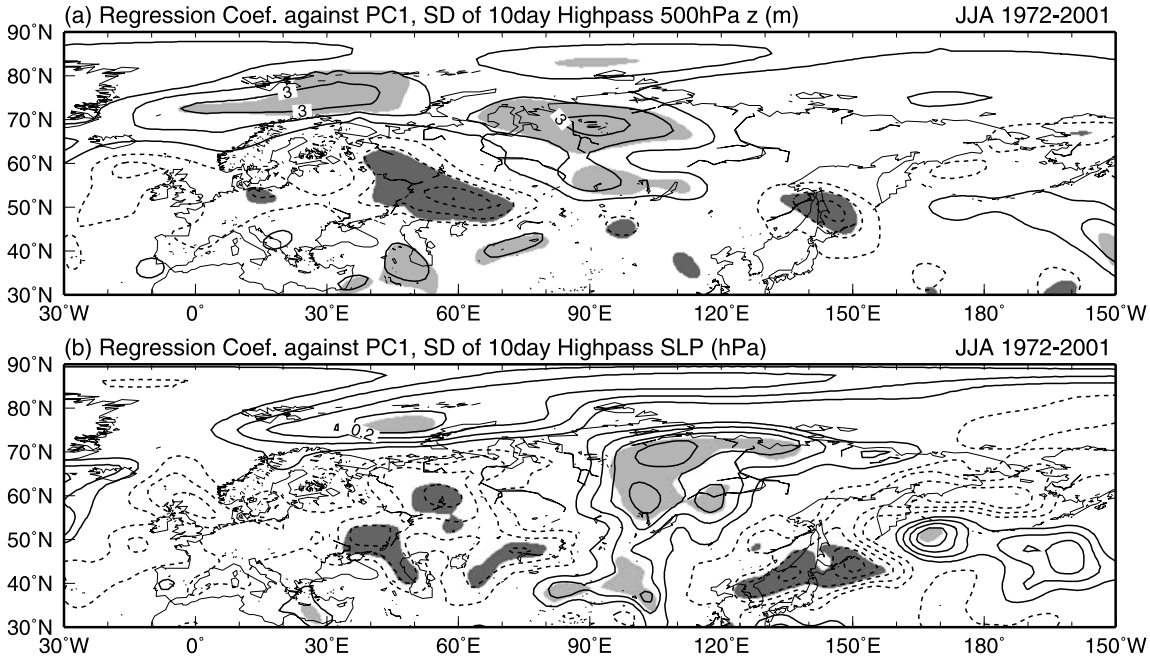

Figure 6. (a) Regression coefficient of the std dev of 10-day high-pass filtered 500-hPa height with PC1 for JJA 1972–2001. Solid (dashed) contours show the positive (negative) values. Zero contours are omitted. Contour interval is 1 m. Shaded regions show statistically significant at the 95% level. (b) Same as Figure 6a except for the sea level pressure with 0.05 hPa interval.

wave structure for each precipitation extreme. Geopotential height tendency fields for the equations were computed at 300 hPa because past studies have shown that eddy vorticity fluxes generally have stronger amplitudes in the upper troposphere. By contrast, temperature tendencies were estimated at 850 hPa because maximum eddy heat fluxes most likely occur at this level over land. The equations were solved globally using the spherical harmonics transform method (SPHEREPACK 3.0: *Adams and Swartztrauber* [1999]).

[31] Regression patterns of the geopotential height and temperature tendency associated with 10-day high-pass transients projected onto the SPSI are shown in Figure 8. As with the other regression maps, the fields presented are for the positive SPSI phase case. Note that negative (positive) geopotential height tendency in general corresponds to cyclonic (anticyclonic) circulation forcing. The overall pattern of the geopotential height tendencies (Figure 8a) shows a mostly in-phase relationship with the summer stationary waves (Figure 4a) over northern Eurasia. This suggests that barotropic feedback of synoptic-scale eddies onto the mean flow is mostly positive. Cyclonic (anticyclonic) forcing is amplified in regions of enhanced (reduced) eddy activity (Figure 6). Consequently, anomalous cyclonic (anticyclonic) forcing due to eddy vorticity flux convergence reinforces the anomalous cyclonic (anticyclonic) mean flow over central-east (west) Siberia. The regression map of the geopotential height tendency at 700 hPa (not shown) is similar to that at 300 hPa, which indicates that low-level vorticity forcing is in the same sense as that at upper-levels. However, the contribution at 700 hPa is minor; the magnitudes are one-fifth to one-eighth those at 300 hPa.

[32] The temperature tendency pattern (Figure 8b) is mostly out-of-phase with the stationary temperature pattern (Figure 4b). Positive (negative) anomalous eddy heat flux convergence occurs within the negative (positive) stationary temperature anomalies, implying that baroclinic feedback induced by synoptic-scale eddy heat fluxes tends to destroy the anomalous mean thermal structure in the lower troposphere. In other words, the synoptic-scale eddy heat fluxes act to dissipate the baroclinic component of the mean flow. However, the Siberian portion of the anomalous temperature tendency pattern is less organized than the height tendency pattern. Besides areas with 95% significance levels are comparatively small in the temperature tendency pattern.

5.2. Composite Structures in the Two Contrasting Precipitation Extremes

[33] Composite maps showing the spatial structures of the transient eddy forcing terms and stationary waves for each of the two extreme phases were constructed to demonstrate the robust behavior of the synoptic-scale eddy forcing. Figures 9 and 10 contain anomaly composites of the 300-hPa height, 850-hPa temperature, and their tendencies for the high-SPSI and the low-SPSI summers, respectively. An anomaly is defined as a deviation from the 30-yr JJA climatology.

[34] Height anomalies at 300-hPa (Figures 9a and 10a) depict a wavetrain over northern Eurasia, which is a pattern similar to the regressed pattern in Figure 4a. In the high-SPSI phase, the cyclonic (anticyclonic) circulation forcing over central-east (west) Siberia (Figure 9b) is nearly collocated with the anomalous summer mean cyclonic (anticyclonic) circulation (Figure 9a). In the low-SPSI phase, the height tendency anomalies (Figure 10b) and the stationary wave anomalies (Figure 10a) are nearly mirror images of those in the high-SPSI phase. The polarity of anomalous

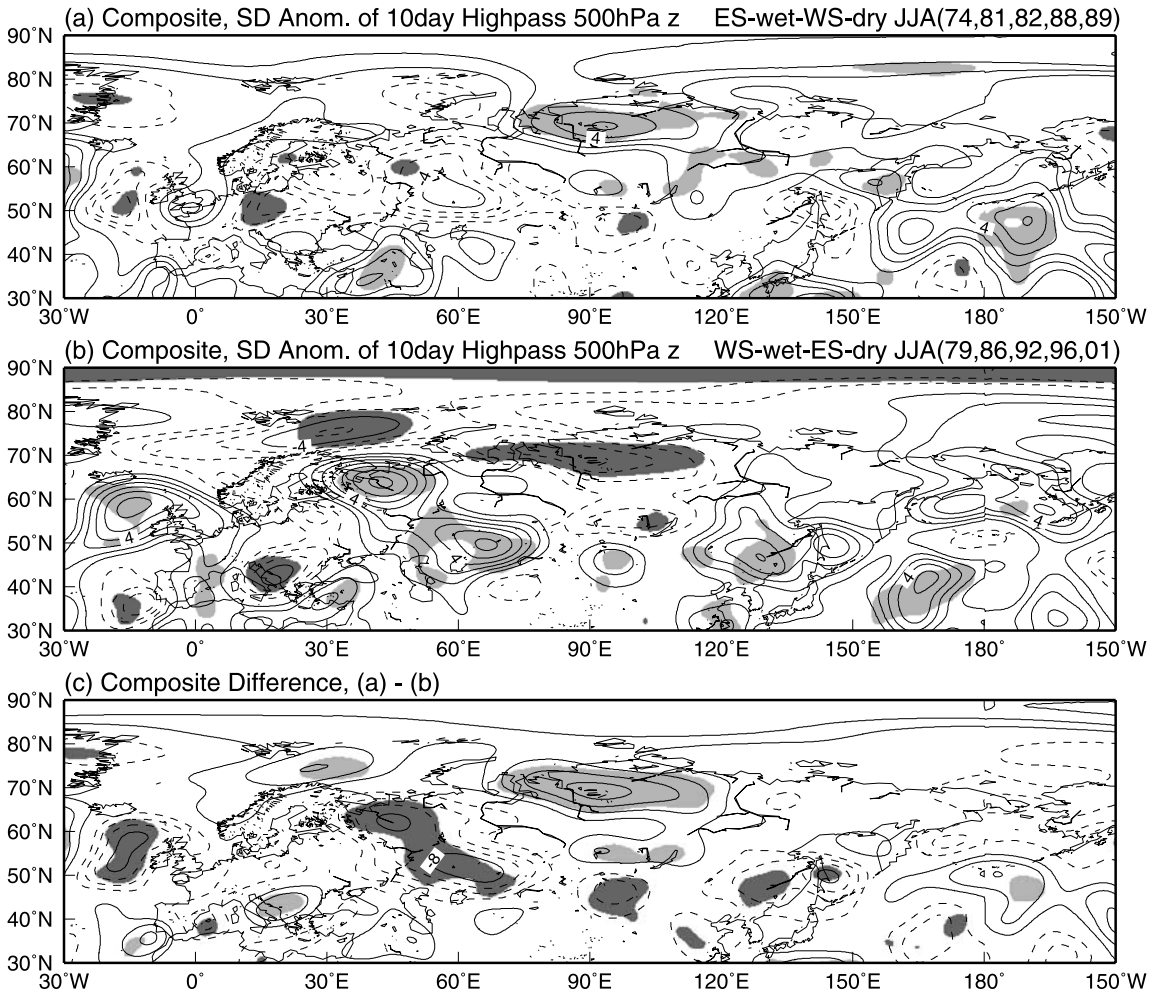

Figure 7. (a) Composite of the std dev. anomalies of 10-day high-pass filtered 500-hPa height defined for the high-SPSI (ES-wet and WS-dry) phases (1974, 1981, 1982, 1988, and 1989). Contour interval is 2 m. Zero contours are omitted. Positive (negative) anomalies statistically significant at 90% level are lightly (darkly) shaded. (b) Same as Figure 7a except for the low-SPSI (WS-wet and ES-dry) phases (1979, 1986, 1992, 1996, and 2001). (c) Composite difference between the two phases. Contour interval is 4 m.

forcing and stationary waves is almost the same. The cyclonic and anticyclonic circulation forcings over Eurasia are collocated with the cyclonic and anticyclonic circulations. Vorticity forcing due to synoptic-scale eddies helps maintain the anomalous stationary wave pattern in both phases.

[35] Temperature anomalies at 850 hPa (Figures 9c and 10c) also show good agreement with the regressed pattern (Figure 4b). Strong anomalous eddy heat fluxes overlie anomalous troughs and ridges. The thermal forcing patterns associated with these heat fluxes (Figures 9d and 10d) are rather noisy, although they account for basic features of the regressed temperature tendency pattern (Figure 8b). In the ES-wet-WS-dry case (Figures 9c and 9d), cooling tendency anomalies well collocate with the summer mean warm anomalies for the WS domain. On the other hand, warming tendency anomalies are not distributed homogeneously in the summer mean cold anomalies for the ES domain. Cooling and warming tendency anomalies in the mean warm and cold anomalies have complex structures also in the WS-wet–ES-dry case (Figures 10c and 10d). Maximum and minimum centers of the tendency anomalies do not coincide with those of the mean temperature anomalies for both the ES and WS domain. Overall, the synoptic-scale baroclinic damping effect on the summer mean temperature anomalies associated with the precipitation dipole seems to be more complicated and less straightforward. Case-to-case variation presumably produces the noisy composite structures.

6. Summary and Discussion

[36] In this study, we identified changes in storm track activity and how the changes affect the seasonal mean flow over northern Eurasia that is associated with an interannual seesaw in summer precipitation between east and west Siberia. In the two extreme phases of this seesaw, an east-west dipole pattern of precipitation anomalies prevails over much of Siberia (Figure 2). We focused on the 30 years from 1972–2001 when such spatial-temporal

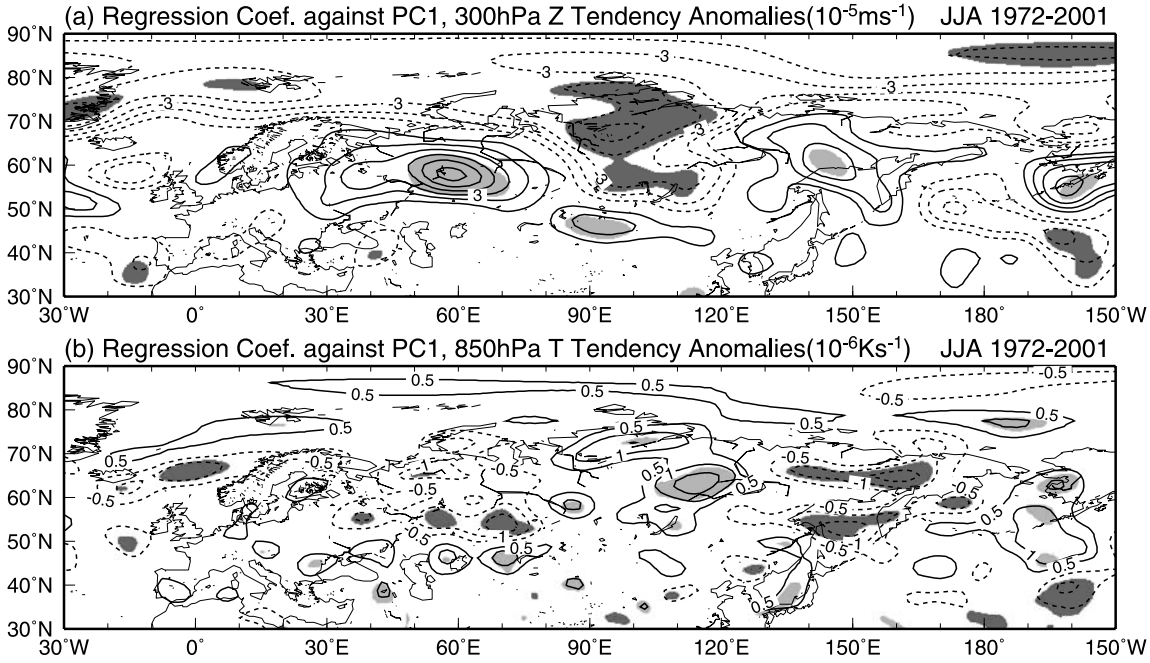

Figure 8. (a) Regression coefficient of the 300-hPa height tendencies due to the synoptic-scale eddy vorticity forcing with PC1 for JJA 1972–2001. Solid (dashed) contours show the positive (negative) values. Zero contours are omitted. Contour interval is 1.0×10^{-5} m s^{-1}. Zero contours are omitted. Shaded regions show statistically significant at the 95% level. (b) Same as Figure 8a except for the 850-hPa temperature tendencies. Contour interval is 0.5×10^{-6} K s^{-1}.

characteristics are clear and consistent (Figure 1c), as noted by *Fukutomi et al.* [2003]. The two precipitation extreme phases that are manifest as out-of-phase dipole patterns are represented as the ES-wet-WS-dry phase and the WS-wet-ES-dry phase. We documented large-scale atmospheric patterns and storm track activities associated with these contrasting phases using linear regression and compositing, and highlighted the synoptic-scale eddy forcing on the mean circulations.

[37] Atmospheric circulation and temperature anomalies related to the precipitation seesaw (Figures 3a, 3b, 9a, 9c, 10a, and 10c) show a clear stationary wavetrain extending from western Eurasia to the North Pacific. The Eurasian dipole pattern at the upstream portion of the wavetrain occurs in conjunction with the precipitation dipole. A cold trough and warm ridge correspond to the relatively wet and dry regions. Regression and composite analyses for the transient eddy statistics (Figures 6 and 7) indicate that anomalous storm track displacement is accompanied by phase reversals between two phases. The ES-wet-WS-dry (WS-wet-ES-dry) phase is associated with intensification of storm track activity over central-east (west) Siberia, and a weakening of storm track activity over west (east) Siberia. The pair of enhanced and reduced storm track activity is collocated with the Eurasian wave pattern during summer. The anomalous stationary trough (ridge) corresponds to a high-(low-)eddy-activity region in each of two phases. In addition, the high (low) eddy activity roughly coincides with the cyclonic (anticyclonic) circulation forcing (Figures 8, 9b, and 10b). These spatially coherent relationships suggest that storm track feedback reinforces and maintains the Eurasian wave structure coupled with the dipole precipitation pattern of each phase. Consequently, the interannual variability of the Eurasian storm track intensity and location is a crucial factor controlling the alternation in mean precipitation and circulation patterns between the two phases.

[38] We have stressed that the east-west displacement of storm track activity can reinforce and maintain the Eurasian stationary waves associated with the two contrasting summer precipitation extreme phases. For both the two phases, barotropic and baroclinic eddy feedback on the stationary waves over northern Eurasia is observed. The barotropic feedback due to eddy vorticity fluxes reinforces the mean circulation structures. This eddy-mean phase relation is analogous to those occurring over the oceanic storm track region, as derived in several works [e.g., *Lau and Nath*, 1991; *Trenberth and Hurrell*, 1994; *Hurrell and van Loon*, 1997; *Sheng et al.*, 1998]. The baroclinic feedback due to eddy heat fluxes seems to dampen the mean thermal structures (baroclinicity) of the lower troposphere. Nevertheless, it is not easy to give a straightforward interpretation as done by these previous studies for oceanic storm tracks because of the complicated distribution of the synoptic-scale eddy heat flux convergence in the present results.

[39] The stationary wavetrains do not originate upstream. Basin-scale precipitation in Siberia does not exhibit any dominant covariance with the Atlantic signals. This suggests much weaker relationships between Atlantic variability and the northern Eurasian summer mean flow linked to this dipole precipitation variability. This conclusion is further supported by poor coherence between the north Atlantic sea surface temperature and northern Eurasian

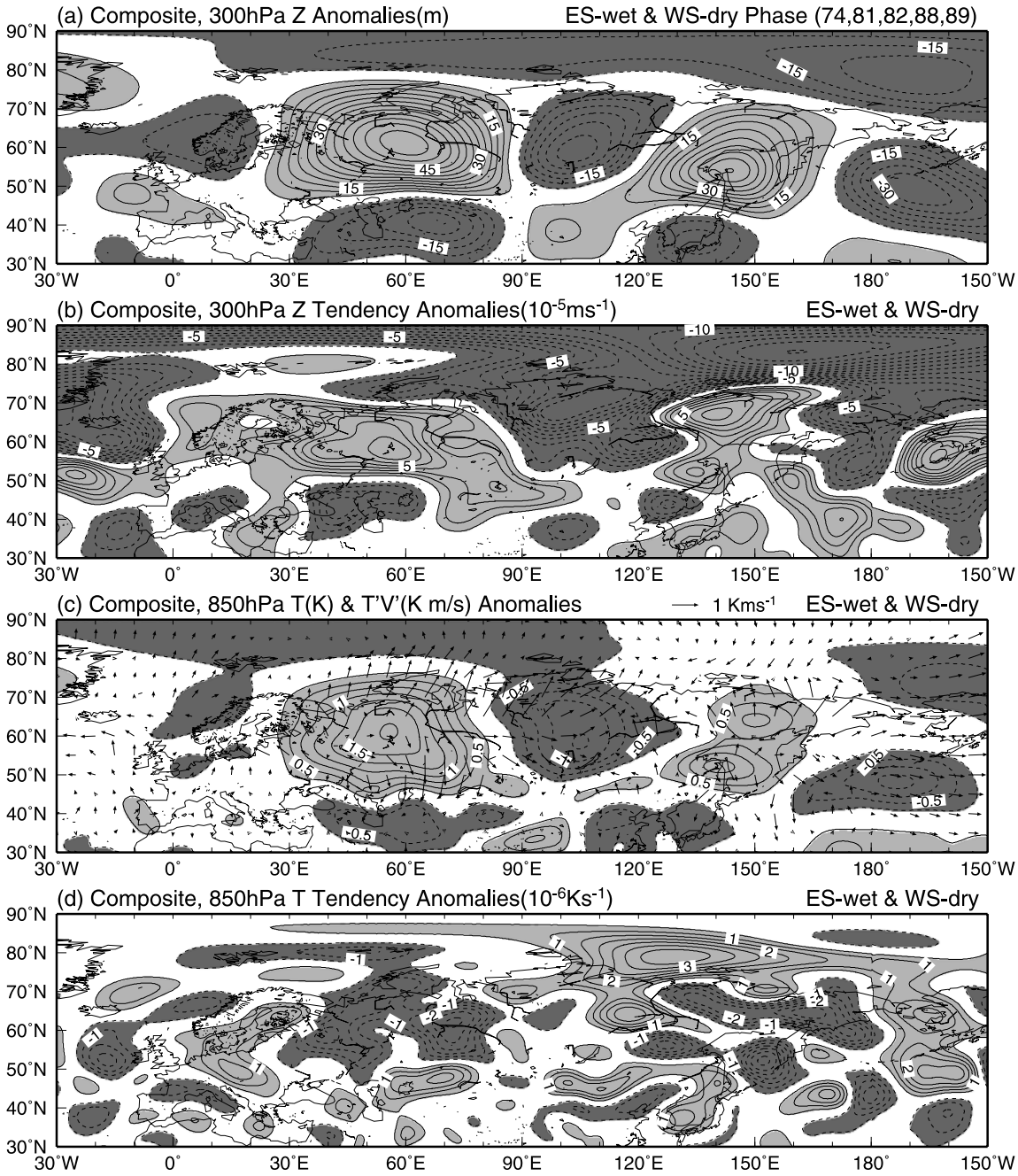

Figure 9. Composites for the high-SPSI (ES-wet and WS-dry) phases. Regions with positive (negative) values are lightly (darkly) shaded. Zero contours are omitted. (a) The 300-hPa height anomalies. Contour interval is 5 m. (b) The 300-hPa height tendencies due to the synoptic-scale eddy vorticity forcing. Contour interval is 5.0×10^{-5} m s^{-1}. (c) The 850-hPa temperature anomalies and the anomalous vectors of synoptic-scale eddy heat flux. Contour interval is 1 K. (d) The 850-hPa temperature tendencies due to synoptic-scale eddy thermal forcing. Contour interval is 0.5×10^{-6} K s^{-1}.

atmospheric circulations for JJA, as shown by *Lin and Derome* [2003, Figure 7]. Accordingly, anomalous wave patterns can be interpreted in an average sense as primarily a response to storm track feedback involving possibly diabatic heating effects induced by synoptic-scale activity, rather than geographically-fixed external forcing in the upstream. However, this interpretation does not preclude the coexistence of other forcing mechanisms accounting for wave patterns in individual cases. Further investigation of the respective elements that support Eurasian stationary waves during summer as proposed by *Park and Schubert* [1997] is needed.

[40] The causes of the interannual variability in the storm track activity that determines the Siberian precipitation dipole are still unresolved. Northern Eurasian storm tracks lie in the Arctic frontal zone where there are sharp meridional gradients in the lower tropospheric temperature [*Serreze et al.*, 2001]. *Serreze et al.* [2001] suggested that

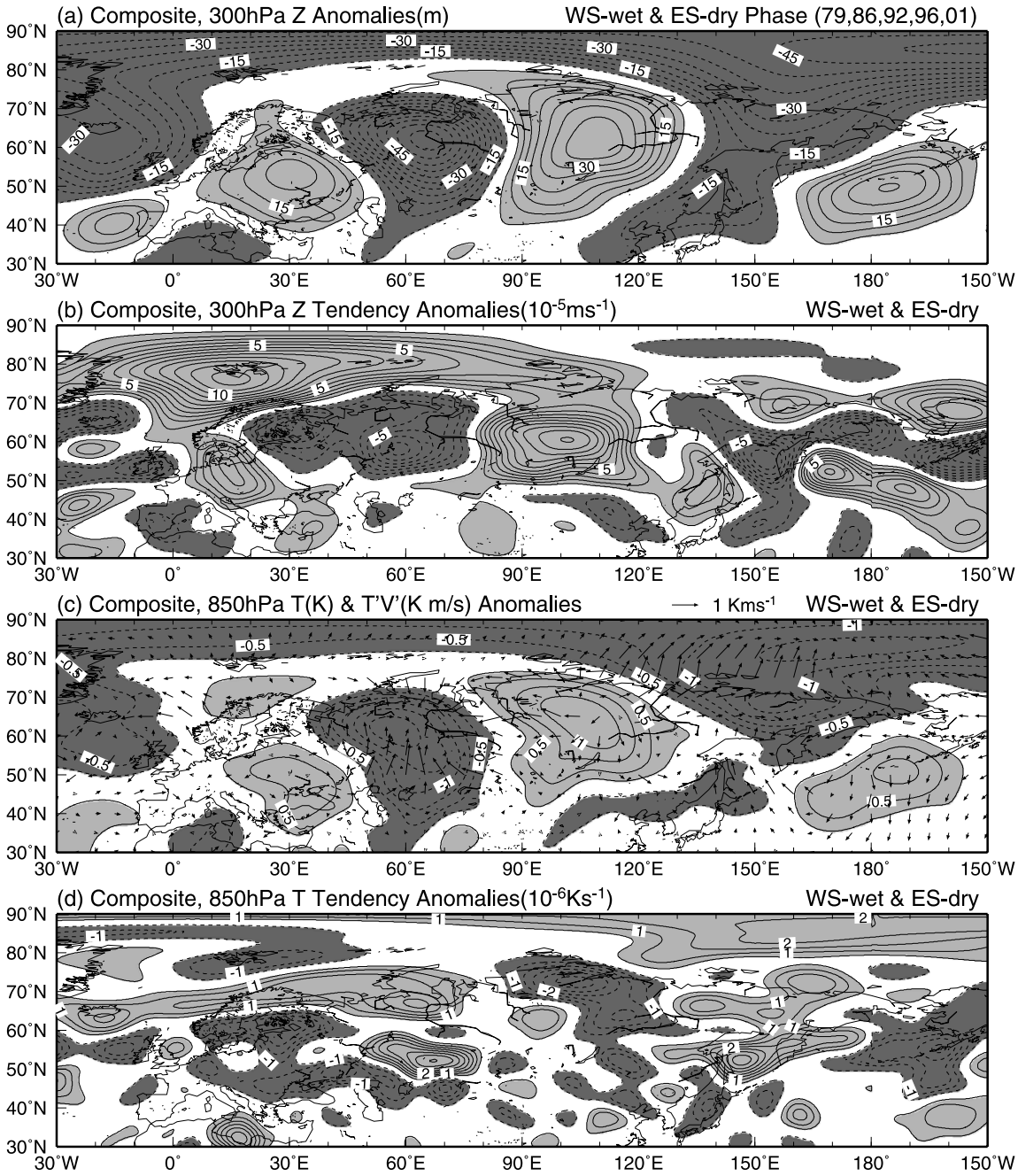

Figure 10. Same as Figure 9 except for the low-SPSI (WS-wet and ES-dry) phases.

the Arctic frontal zone in a climatological sense is supported by differential surface heating between land covered by boreal forest/tundra and the Arctic Ocean. Recent studies suggest that air-land energy exchange and topography maintain the baroclinicity over Alaska [e.g., *Pielke and Vidale*, 1995; *Lynch et al.*, 2001]. However, how such factors vary from summer to summer and how they affect the atmosphere-land interaction in northern Eurasia remains unclear.

[41] Extensive work is required to document all the factors that modulate summer storm track activity and the resulting dynamics over northern Eurasia. One simple approach is to identify regional modes of storm track variability [e.g., *Lau*, 1988; *Rogers*, 1997; *Chang and Fu*, 2002]. Then, the underlying dynamic and thermodynamic processes that locally shift or intensify storm track activities can be examined.

[42] **Acknowledgments.** We wish to thank three anonymous reviewers for constructive comments on an earlier version of this manuscript. Helpful discussions with Hiromichi Igarashi (FRSGC/JAMSTEC) are also appreciated. The PREC/L data set was obtained from the NOAA/CPC (ftp://ftp.ncep.noaa.gov). The NCEP-NCAR reanalysis data set was taken from the NOAA/CDC (ftp://ftp.cdc.noaa.gov). The Generic Mapping Tools (GMT) graphics package outlined by *Wessel and Smith* [1995] was used for drawing all the figures.

References

Adams, J. C., and P. N. Swartztrauber (1999), SPHEREPACK 3.0: A model development facility, *Mon. Weather. Rev.*, *127*, 1872–1878.

Blackmon, M. L. (1976), A climatological spectral study of the 500 mb geopotential height of the Northern Hemisphere, *J. Atmos. Sci.*, *33*, 1607–1623.

Blackmon, M. L., and G. H. White (1982), Zonal wavenumber characteristics of the Northern Hemisphere transient eddies, *J. Atmos. Sci.*, *39*, 1985–1998.

Chang, E. K. M., and Y. Fu (2002), Interdecadal variations in Northern Hemisphere winter storm track intensity, *J. Clim.*, *15*, 642–658.

Chang, E. K. M., and D. B. Yu (1999), Characteristics of wave packets in the upper troposphere. Part II: Seasonal and hemispheric variations, *J. Atmos. Sci.*, *52*, 1729–1747.

Chen, M., P. Xie, J. E. Janowiak, and P. A. Arkin (2002), Global land precipitation: A 50-yr monthly analysis based on gauge observations, *J. Hydrometeorol.*, *3*, 249–266.

Chen, S. J., Y.-H. Kuo, P.-Z. Zhang, and Q.-F. Bai (1991), Synoptic climatology of cyclogenesis over east Asia, 1958–1987, *Mon. Weather Rev.*, *119*, 1407–1418.

Fukutomi, Y., H. Igarashi, K. Masuda, and T. Yasunari (2003), Interannual variability of summer water balance components in three major river basins of northern Eurasia, *J. Hydrometeorol.*, *3*, 249–266.

Hurrell, J. (1995), Transient eddy forcing of the rotational flow during northern winter, *J. Atmos. Sci.*, *52*, 2286–2301.

Hurrell, J., and H. van Loon (1997), Decadal variations in climate associated with the North Atlantic Oscillation, *Clim. Change*, *36*, 301–326.

Kalnay, E., et al. (1996), The NCEP/NCAR 40-year reanalysis project, *Bull. Am. Meteorol. Soc.*, *77*, 437–471.

Kaylor, R. E. (1977), Filtering and decimation of digital time series, *Tech. Note BN850*, 42 pp., Inst. of Phys. Sci. and Technol., Univ. of Md., College Park.

Kistler, R., et al. (2001), The NCEP/NCAR 50-year reanalysis: Monthly means CD-ROM and documentation, *Bull. Am. Meteorol. Soc.*, *82*, 247–268.

Klasa, M., J. Derome, and J. Sheng (1992), On the interaction between the synoptic-scale eddies and the PNA teleconnection pattern, *Beitr. Phys. Atmos.*, *65*, 211–222.

Lau, N.-C. (1988), Variability in the observed midlatitude storm tracks in relation to low-frequency changes in the circulation pattern, *J. Atmos. Sci.*, *45*, 2718–2743.

Lau, N.-C., and E. O. Holopainen (1984), Transient eddy forcing of the time-mean flow as identified by geopotential tendencies, *J. Atmos. Sci.*, *41*, 313–328.

Lau, N.-C., and M. J. Nath (1991), Variability of the baroclinic and barotropic transient eddy forcing associated with monthly changes in the midlatitude storm tracks, *J. Atmos. Sci.*, *48*, 2589–2613.

Lin, H., and J. Derome (2003), The atmospheric response to North Atlantic SST anomalies in seasonal prediction experiments, *Tellus, Ser. A*, *55*, 193–207.

Lynch, A. H., A. G. Slater, and M. C. Serreze (2001), The Alaskan Arctic frontal zone: Forcing by orography, coastal contrast, and the boreal forest, *J. Clim.*, *14*, 4351–4362.

Park, C.-K., and S. D. Schubert (1997), On the nature of the 1994 East Asian summer drought, *J. Clim.*, *10*, 1056–1070.

Pielke, R. A., and P. L. Vidale (1995), The boreal forest and the polar front, *J. Geophys. Res.*, *100*(12), 25,755–25,758.

Raphael, M. N. (1997), The relationship between the transient, meridional eddy sensible and latent heat flux, *J. Geophys. Res.*, *102*(D12), 13,487–13,494.

Rogers, J. C. (1997), North Atlantic storm track variability and its association to the North Atlantic Oscillation and climate variability of Northern Europe, *J. Clim.*, *10*, 1635–1645.

Serreze, M. C. (1995), Climatological aspects of cyclone development and decay in the Arctic, *Atmos. Ocean*, *33*, 1–23.

Serreze, M. C., A. H. Lynch, and M. P. Clark (2001), The Arctic frontal zone as seen in the NCEP-NCAR reanalysis, *J. Clim.*, *14*, 1550–1567.

Serreze, M. C., D. H. Bromwich, M. P. Clark, A. J. Etringer, T. Zhang, and R. Lammers (2003), Large-scale hydro-climatology of the terrestrial Arctic drainage system, *J. Geophys. Res.*, *108*(D2), 8160, doi:10.10,129/2001JD000919.

Sheng, J., J. Derome, and M. Klasa (1998), The role of transient disturbances in the dynamics of the Pacific-North American pattern, *J. Clim.*, *11*, 523–536.

Ting, M., and N.-C. Lau (1993), A diagnostic and modeling study of the monthly mean wintertime anomalies appearing in a 100-year GCM experiment, *J. Atmos. Sci.*, *50*, 2845–2867.

Trenberth, K. E. (1991), Storm tracks in the Southern Hemisphere, *J. Atmos. Sci.*, *48*, 2159–2178.

Trenberth, K. E., and J. W. Hurrell (1994), Decadal atmosphere-ocean variations in the Pacific, *Clim. Dyn.*, *9*, 303–319.

Wallace, J. M., G. H. Lim, and M. L. Blackmon (1988), Relationship between cyclone tracks, anti-cyclone tracks, and baroclinic waveguides, *J. Atmos. Sci.*, *45*, 439–462.

Walsh, J. E. (2000), Global atmospheric circulation patterns and relationships to Arctic freshwater fluxes, in *The Freshwater Budget of the Arctic Ocean*, edited by E. L. Lewis et al., pp. 21–43, Kluwer Acad., Norwell, Mass.

Wessel, P., and W. H. F. Smith (1995), New version of the Generic Mapping Tools released, *Eos Trans. AGU*, *76*(33), 329.

White, G. H. (1982), An observational study of the Northern Hemisphere extratropical summertime general circulation, *J. Atmos. Sci.*, *39*, 24–40.

Whittaker, L. M., and L. H. Horn (1984), Northern Hemisphere extratropical cyclone activity for four mid-season months, *J. Climatol.*, *4*, 297–310.

Yang, D., D. L. Kane, L. D. Hinzman, X. Zhang, T. Zhang, and H. Ye (2002), Siberian Lena river hydrologic regime and recent change, *J. Geophys. Res.*, *107*(D23), 4694, doi:10.1029/2002JD002542.

Ye, H. (2002), Observed regional and climatological associations between spring and summer precipitation over northern central Eurasia, *Water Resour. Res.*, *38*(12), 1317, doi:10.1029/2001WR001060.

Y. Fukutomi, K. Masuda, and T. Yasunari, JAMSTEC Yokohama Institute for Earth Sciences, 3173-25 Showamachi Kanazawa-ku, Yokohama, Kanagawa, 236-0001, Japan. (fukutomi@jamstec.go.jp)